JOURNAL OF MATERIALS SCIENCE 33 (1998) 4477–4483

# Precipitation kinetics in Al6061 and in an Al6061-alumina particle composite

S. P. CHEN, K. M. MUSSERT, S. VAN DER ZWAAG
*Laboratory for Materials Science, Delft University of Technology, Rotterdamseweg 137, 2628 AL Delft, The Netherlands*

Differential scanning calorimetry (DSC) was used to study the precipitation kinetics of metastable phases in an Al6061 alloy and a 20 vol % alumina particle reinforced Al6061 composite. The thermal effects in the DSC traces were analysed quantitatively. The kinetic parameters for the phase transformations in the Al6061 alloy and composite were calculated using the varying heating rate method and the Kissinger approach. It was found that the overall age-hardening sequence of the Al6061 alloy did not change due to the addition of $Al_2O_3$ particles, but the volume fractions of the various phases and the precipitation kinetics of some of the phases were modified. The precipitation transformations of the metastable phases in both the Al6061 and the composite obey an *n*-order kinetic model. © *1998 Kluwer Academic Publishers*

## 1. Introduction

Aluminium-based metal matrix composites (MMCs) reinforced with ceramic particles are attractive because of their improved mechanical properties due to synergetic effects between the matrix and the reinforcement [1]. The aluminium matrix is often of the precipitation hardenable type, responding to a solutionize–quench–age heat treatment. It is likely that the mechanical properties of the matrix alloy play a significant role in the strength of the composite. It has been reported that increase in strength in an Al6061 alloy due to age hardening is positively affected by the introduction of 20 vol % SiC particles [2, 3]. However, reinforcements such as $Al_2O_3$ and SiC are not thought to affect the overall chemistry of the matrix. Hence, the reinforcing particles must affect the precipitation response in the matrix. This stimulation of the precipitation process is attributed to vacancy annihilation and a high dislocation density resulting from differential thermal expansion as well as stimulated nucleation at the particle–matrix interface. It is evident that precipitation hardening behaviour must be studied in order to optimize the properties of the MMCs.

Al6061, a widely used typical extrusion alloy containing Mg and Si as the principal alloying elements, is a very suitable alloy as matrix for MMCs. The precipitation processes in Al6xxx alloys are more complicated than those in Cu bearing Al2xxx alloys, since the formation of metastable phases requires diffusion of both Mg and Si. Although there are some reports about the precipitation sequence and kinetics in Al6xxx alloys [3–6], the exact order is not known as different results have been reported thus far. Edwards *et al.* [5] proposed that the precipitation sequence in an Al–Mg–Si alloy consists of the formation of separate clusters of Mg and Si atoms, co-clusters of Mg and Si atoms, small equiaxed precipitates, β″ precipitates, β′ and B′ precipitates and, finally, β-$Mg_2Si$ precipitates. Dutta and Allen [6] found the precipitation processes in an Al6061 alloy to be associated with vacancy-silicon clusters, GP-I zone, GP-II zone, β′ and β-$Mg_2Si$ formation. Papazian [3] did not find clusters or GP-zones in Al6061. So the precipitation processes in Al6061 alloys and their kinetics remain largely unknown.

In light of the reasons described above, and of the emerging awareness of the importance of the microstructure of the matrix for MMC properties, it is thought that an investigation of the precipitation kinetics of an Al6061 alloy and the effects of $Al_2O_3$ reinforcements on the kinetics would be appropriate. Differential scanning calorimetry (DSC) was selected as the principal technique, because this allows rapid but accurate evaluation of the kinetics of the various reactions taking place in the base material and the $Al_2O_3$ particle-reinforced material.

### 1.1. Kinetic analysis

A DSC run yields the heat flow (heat release or absorption), $dH/dt$, due to a phase transformation as a function of temperature under a constant heating rate. The partial area divided by the total area, $A$, under a DSC peak is taken as equal to the fraction, $y$, of the transformation completed at a given time, thus

$$y = \frac{1}{A}\int_0^t \frac{dH}{dt}dt \tag{1}$$

or in differential form

$$\frac{dH}{dt} = A\frac{dy}{dt} \tag{2}$$

Hence, dividing the partial DSC output by the area under the peak results in a plot of $dy/dt$, which is a convenient function to fit to the kinetic equations. Many studies [7–9] have shown that the results of continuous heating experiments can be used to obtain a good kinetic description of the process by assuming that the rate of transformation is given by

$$\frac{dy}{dt} = k(T)f(y) \tag{3}$$

where $k(T)$ is the rate constant defined as $k(T) = k_0 \exp(-E/RT)$, where $k_0$, $R$ and $T$ denote the pre-exponential factor, the gas constant and the absolute temperature, respectively, and $E$ is the activation energy. $f(y)$ is a function depending on the reaction mechanism of the transformation. In heterogeneous solid-state transformations, $f(y)$ is often approximated by an $n$-order kinetic model [7, 10, 11]

$$f(y) = n(1-y)\left[\ln\left(\frac{1}{1-y}\right)\right]^{[(n-1)/n]} \tag{4}$$

That is, the kinetics of heterogeneous solid-state transformations under non-isothermal conditions can be described by an equation

$$y = 1 - \exp[-(\beta)^n] \tag{5}$$

where $n$ is a numerical exponent, $\beta = \int k(T)\,dt$ is the state variable fully determining the state of transformation. In non-isothermal transformations, $T$ and $k(T)$ depend on $t$. There are several ways to extract the kinetic parameters from Equation 3. For a constant heating rate $\phi = dT/dt$, after rearranging Equation 3, we get the following expression for the relation between the rate of transformation and the activation energy of the process

$$\ln\left[\left(\frac{dy}{dT}\right)_{y_i}\phi_j\right] = \ln[f(y)k_0] - \left(\frac{E}{R}\right)\frac{1}{T_j} \tag{6}$$

where $y_i$ is the fraction transformed for all reactions taking place at temperature, $T_j$, when the heating rate is $\phi_j$. A plot of $\ln[(dy/dT)_{y_i}\phi_j]$ against $(1/T_j)$ should yield a straight line of slope $(-E/R)$, from which the value of the activation energy of the process can be calculated without recourse to any special model for the transformation kinetics.

Mittemeijer and co-workers [12, 13] used the so-called Kissinger-like method to extract kinetic parameters from data obtained in non-isothermal experiments. Using an approximation to the integral $\beta = \int k(T)\,dt \approx (T^2/\phi)(R/E)k$, the following expression was derived for a fixed stage of transformation, $y_f$

$$\ln\frac{T_{y_f}^2}{\phi} = \frac{E}{RT_{y_f}} + \ln\frac{E}{Rk_0} + \ln\beta_{y_f} \tag{7}$$

They further showed that the temperature, $T_i$, where the reaction rate has a maximum (i.e. the temperature corresponding to the point of inflection on the $y$–$T$ curve), is an appropriate substitute for $T_{y_f}$, the temperature for a fixed stage of transformation. It has been shown [12] that for non-isothermal kinetics $\beta_{T_i} \cong 1$, so the last term in Equation 7 could be neglected without incurring significant error. The slope of the plot of $\ln(T_i^2/\phi)$ against $(1/T_i)$ yields the activation energy.

For precipitation transformations that are partially superimposed, we assume that the heat release detected by the calorimeter may be taken as the sum of the heat flows of each transformation, thus

$$\frac{dH}{dt} = \frac{dH_1}{dt} + \frac{dH_2}{dt} \tag{8}$$

Combining Equations 2 and 8 and $\phi = dT/dt$, results in

$$\frac{dH}{dt} = A_1\frac{dy_1}{dT} + A_2\frac{dy_2}{dT} \tag{9}$$

Using Equation 5 and taking $\beta_i = (T^2/\phi)(R/E_i)k_{0_i}\exp(-E_i/RT)$ we obtain

$$\frac{dy_i}{dT} = n_i\beta_i\exp(-\beta_i^{n_i})\left(\frac{2}{T} + \frac{E_i}{RT^2}\right) \tag{10}$$

Combining Equations 9 and 10, the coefficients $A_i$, $n_i$, $k_{0_i}$ and $E_i$ can be determined from the DSC trace by using the non-linear regression version of Marquart's method of minimization of least squares error of experimental data to Equation 9, upon reasonable estimations of the initial values.

## 2. Experimental procedure

The alloy Al6061 and the composite Al6061 + 20 vol % $Al_2O_3$ used in the experiments were manufactured using powder metallurgy, followed by extrusion. The compositions of Al6061 and the composite materials, as listed in Table I, were measured using X-ray fluorescence (XRF).

Samples for DSC analysis in the form of discs 6 mm in diameter by 0.8 mm thickness, with an approximate weight of 46 mg, were cut from the extruded rod and were solution treated at 530 °C for 1 h in air, followed by quenching into water at 12 °C (WQ). Then, the discs were examined immediately in a Perkin-Elmer DSC7 over a temperature interval ranging from 0 to 530 °C using a set of heating rates up to 40 °C min$^{-1}$. Dry nitrogen was passed through the cell to avoid oxidation. Efforts were made to ensure that the delay between WQ treatment and DSC analysis was as short as possible. For comparison, water quenched samples, stored in a fridge for various periods were also analysed. Typically, at least three DSC samples were made for each heat treatment condition. The results obtained were found to be highly reproducible. Al6061 and/or composite samples aged for 10 h at 400 °C with a mass close to that of the specimen were found to be very suitable as reference materials. The baselines were obtained by subtracting the output of the reference measurements from that of the specimen.

TABLE I Chemical composition (wt %) of the materials tested

| Material | Mg | Si | Cu | Ni | Mn | Cr | Fe | Ti |
|---|---|---|---|---|---|---|---|---|
| Al6061 | 0.890 | 0.628 | 0.338 | 0.011 | 0.104 | 0.104 | 0.364 | 0.030 |
| MMC | 1.107 | 0.446 | 0.229 | 0.006 | 0.001 | 0.029 | 0.045 | 0.012 |

## 3. Results and discussion

### 3.1. Differential scanning calorimetry

The DSC thermograms, as shown in Fig. 1, were obtained at heating rates of 5, 10, 20 and 40 °C min$^{-1}$ over the range 0–530 °C. The average peak temperatures and the heat effects associated with these transformations are shown in Tables II and III, respectively. For the solutionized and freshly quenched Al6061 the traces show that there are four exothermic peaks in the interval 0–530 °C. For a heating rate of 10 °C min$^{-1}$, one peak is at 83 °C (A), two partially overlapping peaks close to 243 °C (B) and 298 °C (C), and one at 495 °C (D).

Furthermore, peak B is found to be a doublet of $B_1$ and $B_2$. All peaks are found to shift to lower temperatures at lower heating rates, indicating that the rate of formation is controlled by the reaction kinetics. In line with other studies [5, 6, 14] the precipitation events in the freshly solutionized and quenched Al6061 are assigned to take place in the following sequences: supersaturated solid solution, vacancy related clusters (exothermic peak A), GP-I and GP-II (β″) zone formation (peak $B_1$, $B_2$), β′ formation (peak C) and β-$Mg_2Si$ formation (peak D).

The calorimetric measurements on the MMC samples show a similar behaviour. The precipitation sequences and the shapes of the peaks do not change, but some aspects of the reactions are altered. The precipitation peaks are slightly advanced to lower temperatures compared with those for monolithic Al6061 at the same heating rate. The area and the height of all peaks are smaller than those of the corresponding peaks in Al6061. As shown in Table II, for a heating rate of 10 °C min$^{-1}$, peak A, peak $B_2$ and peak C shift to lower temperature by 1.2, 2.5 and 7 °C, respectively. The ratios of the volumes of peak A, peak B and peak C in the MMC to those of corresponding peaks in Al6061 are 0.27, 0.81 and 0.54, respectively. The peak ratio for peak β″ (peak $B_2$) should be interpreted in the light of the difference in chemical composition between the Al6061 alloy and the 6061 matrix of the MMC. Using the data provided by reference [15], the maximum volume fractions β″ (peak $B_2$) formed in the same amount as Al6061 and the matrix of the MMC can be calculated to be 1.36 and 1.27 vol %, respectively. Taking into account that the MMC contains 20 vol % $Al_2O_3$, the ratio of the β″ volume fraction in MMC to that in Al6061 should be 0.75 (i.e. $0.8 \times 1.27/1.36$). This is less than the observed ratio of 0.81, which indicates that the presence of $Al_2O_3$ particles promotes the formation of β″. These observations indicate that the addition of a reinforcing phase accelerates ageing of MMC precipitation process relative to the matrix alloy, decreases the volume fractions of peaks A and C, but increases the volume fraction of peak B.

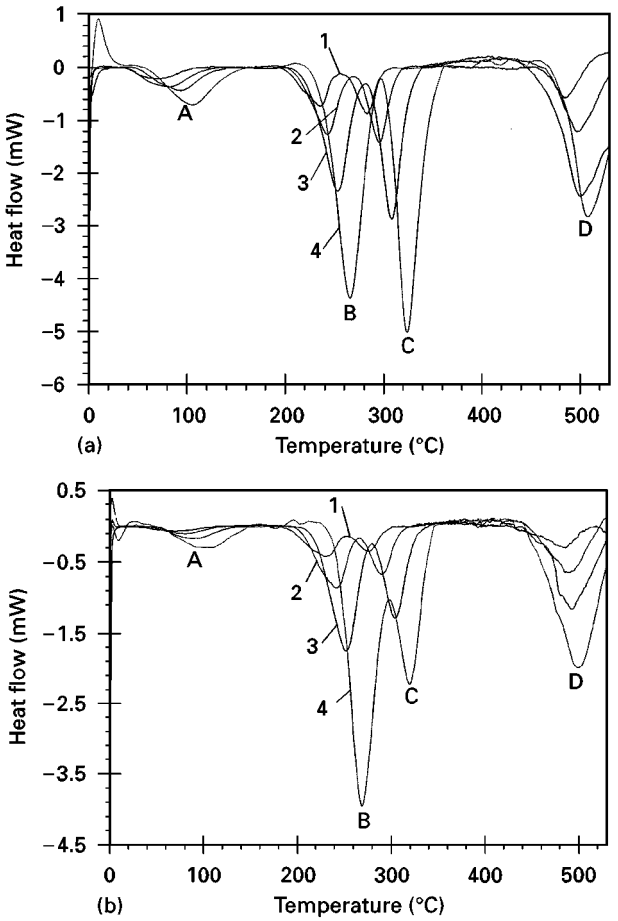


*Figure 1* DSC thermograms for various heating rates, showing four precipitation peaks A through D: (a) as-quenched Al6061 and (b) as-quenched 20 vol % $Al_2O_3$–Al6061(MMC). (1) 5°C/min; (2) 10°C/min; (3) 20°C/min; (4) 40°C/min.

A closer look at the thermograms of both Al6061 and MMC for heating rates of 5 and 10 °C min$^{-1}$ suggests that peak B is an unresolved doublet. As shown in Fig. 2, the peaks B in the DSC traces at low heating rates can be separated with perfect fit for individual peaks to *n*-order reaction kinetics (Equation 4). The doublet cannot be resolved at higher heating rates. Whether peaks $B_1$ and $B_2$ fully overlap or whether one of them disappears with increasing heating rate is still under analysis.

Al6061 and its composite are very sensitive to the delay time between quenching and the DSC

TABLE II DSC peak temperatures (°C) as a function of the heating rate

| Heating rate (°C min$^{-1}$) | Peak A | | Peak $B_1$ | | Peak $B_2$ | | Peak C | |
|---|---|---|---|---|---|---|---|---|
| | Al6061 | MMC | Al6061 | MMC | Al6061 | MMC | Al6061 | MMC |
| 5 | 71.2 | 70.4 | 214.9 | 209.6 | 233.6 | 230.8 | 285.5 | 276.7 |
| 10 | 82.8 | 80.6 | 218.2 | 221.0 | 242.8 | 241.4 | 298.2 | 291.2 |
| 20 | 93.8 | 89.7 | – | – | 253.5 | 252.5 | 308.8 | 304.7 |
| 40 | 105.6 | 102.4 | – | – | 266.3 | 269.1 | 324.2 | 320.5 |

TABLE III Total heat effects (J g$^{-1}$) of the DSC peaks at different heating rates

| Heating rate (°C min$^{-1}$) | Peak A | | Peak B ($B_1 + B_2$) | | Peak C | |
|---|---|---|---|---|---|---|
| | Al6061 | MMC | Al6061 | MMC | Al6061 | MMC |
| 5 | 2.32 | 0.73 | 4.15 | 3.13 | 3.18 | 1.14 |
| 10 | 2.11 | 0.59 | 4.01 | 3.02 | 3.22 | 1.41 |
| 20 | 1.46 | 0.52 | 4.09 | 3.06 | 3.89 | 1.35 |
| 40 | 1.39 | 0.49 | 4.14 | 2.83 | 3.81 | 1.13 |

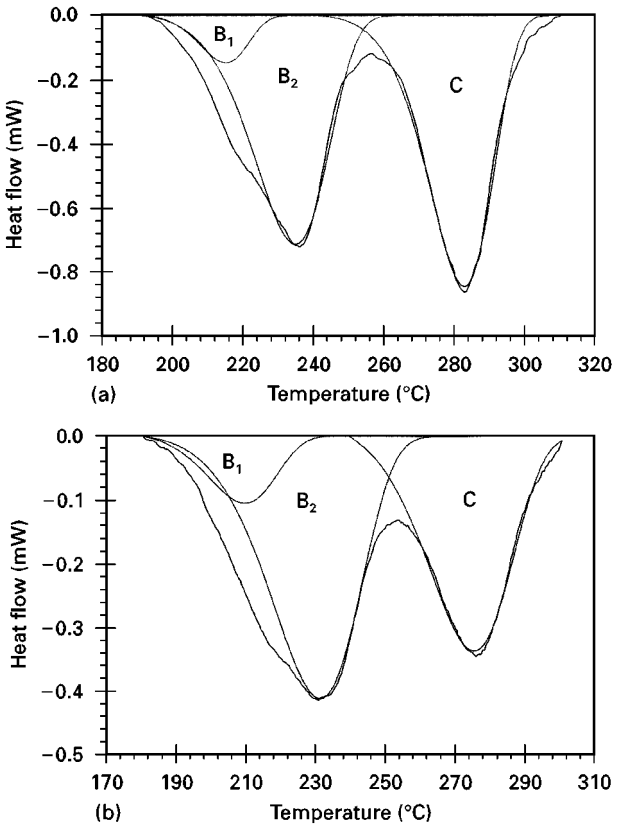


*Figure 2* Part of the DSC traces after deconvolution showing peak B consisting of two unresolved exotherms, $B_1$ and $B_2$ (deconvoluted by equation 10) for a heating rate of 5 °C min$^{-1}$ (a) Al6061 and (b) MMC.

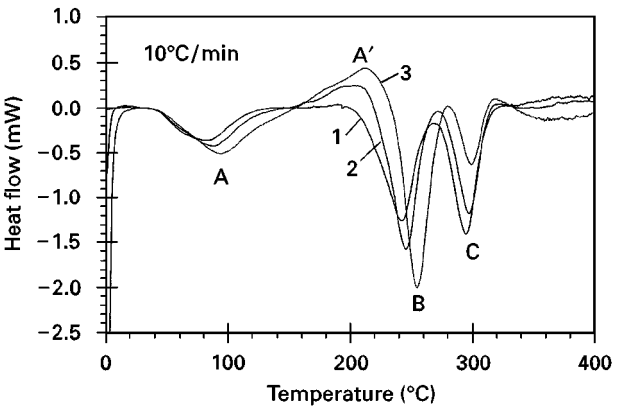


*Figure 3* The effect of delay time in the fridge on the DSC thermograms of Al6061. (1) no delay; (2) delay in fridge for 24 h; (3) delay in fridge for 48 h.

experiments. Samples were stored in a fridge at −5 °C. Fig. 3 shows the effect of the delay time on the DSC runs of Al6061. The peak A temperature shifts to higher temperatures with progressive delay in the fridge, with the onset temperature being unchanged. A delay time leads to the formation of an endothermic peak A′, the longer the delay, the bigger peak A′. Peaks B shifts to higher temperatures and seem to become one peak, $B_2$. The temperature of peak C does not change, but the height of the peak is reduced. These observations indicate that delay supports peak $B_2$ formation but retards the formation of peak C. Similar effects were found for the MMC.

## 3.2. Kinetic parameters for the various phase transformations

### 3.2.1. Varying heating rate method (Equation 6)

The DSC peak designated A in Fig. 1 is assigned to the formation of vacancy-solute clusters. The fraction transformed of the phase, $y$, and the precipitation rate ($dy/dT$), calculated from the DSC peak A using Equations 1 an 2 are shown as a function of temperature in Fig. 4 for Al6061. The $y$–$T$ curves (Fig. 4a) have the expected sigmoidal shape and shift to higher temperatures with increasing heating rate, which implies a kinetically controlled transformation. The data extracted from Fig. 4a and b are replotted in Fig. 5 for four values of $y_i$ (0.2, 0.4, 0.6 and 0.8) using Equation 6. The average slope of the four straight lines obtained from the $(dy/dT)_{y_i}\phi_j]$ versus $(1/T)$ plots yields the activation energy, $E$, for peak A formation.

Similar procedures and plots were used to calculate the activation energies for the transformation processes related to the other peaks. The kinetic parameters obtained for the two materials are summarized in Table IV.

### 3.2.2. Kissinger-like method (Equation 7)

It can be proved that the inflection point temperature, $T_i$, of the $y$ versus $T$ curves is the peak temperature in the DSC experiment. The average values of the peak temperatures for all peaks of the two materials are listed in Table II. By plotting $\ln(T_i^2/\phi)$ against $(1/T_i)$, as shown in Fig. 6, the effective activation energies for peaks in both materials were obtained (see Table IV). These values agree very well with the results obtained from the varying heating rate method (Equation 6). Barring extrapolation errors, the pre-exponential factors, $k_0$, were also calculated.

Kinetic parameters obtained by analysis of the calorimetric signal according to the $n$-order model given by Equation 10 are listed in Table V for heating rates of 5 and 10 °C min$^{-1}$. The good agreement of the

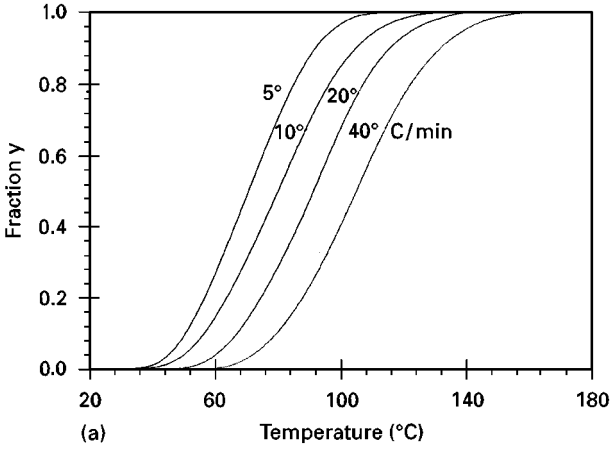


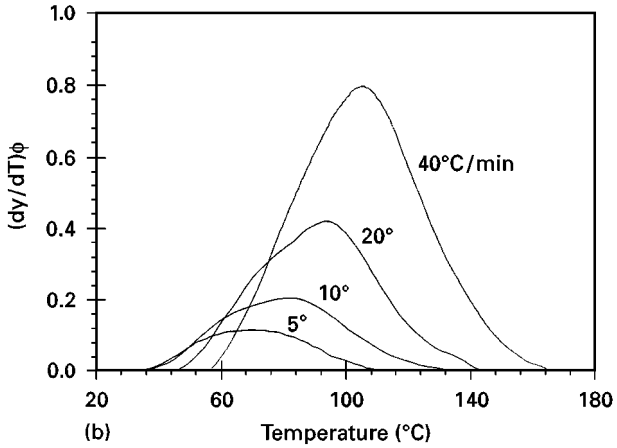


*Figure 4* (a) The $y$ versus temperature curves and (b) $(dy/dT)\phi$ versus temperature, for peak A formation at different heating rates (Al6061).

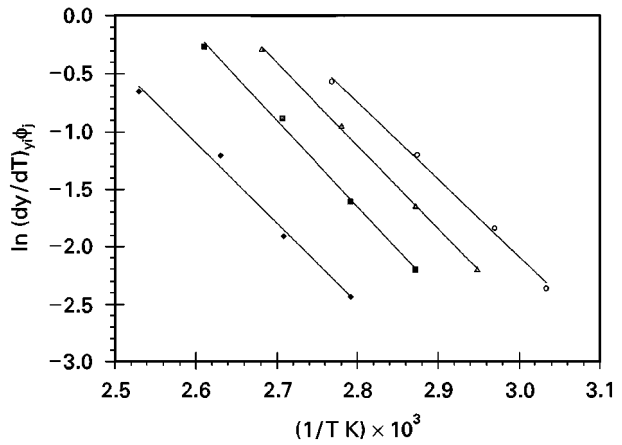


*Figure 5* Plots of $\ln(dy/dT)$ versus the reciprocal temperature for peak A formation in Al6061 (after Equation 6). ◆ $y = 0.8$; ■ $y = 0.6$; △ $y = 0.4$; ○ $y = 0.2$.

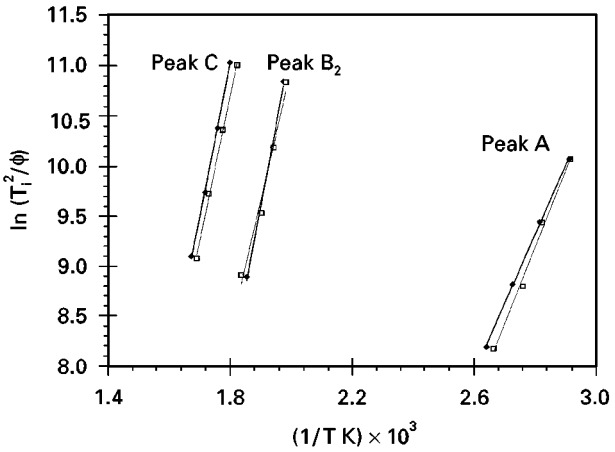


*Figure 6* Arrhenius diagram for phase transformations in Al6061 and MMC: ● = Al6061; □ = MMC.

values between Tables IV and V shows that the phase transformations in Al6061 and MMC follow the $n$-order model, with $n$ varying only modestly between 0.9 and 1.2.

Comparison of the results for Al6061 and MMC shows the following effects.

1. Precipitation of peak A in the composite requires a higher driving force than in the unreinforced alloy.
2. The activation energy required for the precipitation of peak $B_2$ (GP-II) reduces from 135 to 110 kJ mol$^{-1}$ in the composite.
3. The addition of $Al_2O_3$ does not change the activation energies for the formation of peaks $B_1$ and C (within experimental error).

These effects will now be discussed in more detail.

The values of the activation energy for peak A formation obtained in the present study for Al6061 and MMC are 58 and 64 kJ mol$^{-1}$, respectively; and are in the range 41–66.9 kJ mol$^{-1}$, i.e. the migration energy of vacancies in Al–Cu alloys and Al–Cu–Mg alloys [10, 16]. When the alloy is quenched from the solution treatment temperature, excess vacancies are quenched in. In the presence of excess vacancies, diffusion of the solute proceeds at a rate equal to that for migration of the vacancies. Thus, peak A reflects diffusion of vacancies. It is believed that the relatively high dislocation density introduced by differential thermal expansion between the reinforcement and the matrix in the MMCs [4, 17] on quenching from the solution heat treatment temperature influences the precipitation kinetics in a complex manner. First, the dislocations and the particle–matrix interfaces give rise to vacancy annihilation, thus retarding the precipitation

TABLE IV Kinetic parameters for the transformations

| Parameter | Equation | Peak A | | Peak $B_2$ | | Peak C | |
|---|---|---|---|---|---|---|---|
| | | Al6061 | MMC | Al6061 | MMC | Al6061 | MMC |
| E, kJ mol$^{-1}$ | 6 | 60.5 | 65.5 | 129.8 | 114.1 | 123.9 | 122.8 |
| | 7 | 58.1 | 64.1 | 135.2 | 110.1 | 127.5 | 120.4 |
| $k_0$, min$^{-1}$ | 7 | $1.95 \times 10^8$ | $1.86 \times 10^9$ | $2.86 \times 10^{13}$ | $7.06 \times 10^{10}$ | $2.43 \times 10^{11}$ | $6.63 \times 10^{10}$ |

TABLE V Kinetic parameters by simulation according to Equation 10

| Parameter | Heating rate | Peak $B_1$ | | Peak $B_2$ | | Peak C | |
|---|---|---|---|---|---|---|---|
| | | Al6061 | MMC | Al6061 | MMC | Al6061 | MMC |
| E, kJ mol$^{-1}$ | 5 | 92.5 | 93.6 | 127.5 | 110.9 | 127.4 | 126.6 |
| | 10 | 89.7 | 92.1 | 128.4 | 110.1 | 124.7 | 125.8 |
| $k_0$, min$^{-1}$ | 5 | $6.8 \times 10^{11}$ | $6.9 \times 10^{11}$ | $5.8 \times 10^{14}$ | $6.5 \times 10^{12}$ | $4.4 \times 10^{13}$ | $5.0 \times 10^{13}$ |
| | 10 | $7.1 \times 10^{11}$ | $6.8 \times 10^{11}$ | $7.6 \times 10^{14}$ | $5.6 \times 10^{12}$ | $3.1 \times 10^{13}$ | $4.2 \times 10^{13}$ |
| $n$ | 5 | 1.235 | 1.011 | 0.975 | 0.943 | 1.224 | 0.914 |
| | 10 | 1.356 | 1.066 | 0.868 | 0.955 | 1.275 | 0.989 |

process and reducing the volume fraction of the precipitates formed. Second, the high dislocation density and the particle–matrix interfaces act as nucleation sites for heterogeneous nucleation of the precipitation and offer high diffusivity paths for the solute in the composite and so promote the ageing process. Dislocations have been shown by both theoretical and experimental analysis [18] to serve as short-circuits paths for solute diffusion. In fact, at lower temperatures, dislocations can have little effect on the rate of zone formation because few atoms are near a dislocation and dislocations are stationary. With the temperature increasing the effect of dislocations would become more significant. Hence, with the vacancy concentration being lower in the MMCs than in the monolithic alloys, the height of peak A should be lower in the MMC. In a vacancy-deficient environment, the activation energy required for peak A formation would be higher than in the vacancy-rich counterpart. It is to be expected that the activation energy for peak A formation in the MMC is larger than that in the unreinforced alloy.

Comparing the kinetic parameters of peaks $B_1$ and $B_2$, the lower activation energy for peak $B_1$ implies that there is a lower kinetic barrier for its reaction to take place and initially it is the favoured transformation, as observed. The larger pre-exponential factor, often called the frequency factor, for peak $B_2$ implies that the jump rate of atoms across the interface of the $\beta''$ phase is large, so that if the kinetic barrier is surmountable, a comparatively large volume of $\beta''$ will result.

The activation energy for formation of peak $B_1$ is about 90 kJ mol$^{-1}$, which is much lower than the activation energies for migration of Si and Mg. (The activation energies for Si and Mg migration in bulk aluminium are 139 and 110 kJ mol$^{-1}$, respectively [19].) It can be inferred that the formation of peak $B_1$ is associated with vacancy-assisted diffusion of solute atoms. When the heating rate is increased, GP-I (peak $B_1$) formation should be at a higher temperature. However, when the temperature is high enough, the solute atoms get enough energy to surmount the higher kinetic barrier of GP-II, resulting in the formation of GP-II (peak $B_2$) at the expense of peak $B_1$.

The activation energy for peak $B_2$ formation in Al6061 is 135 kJ mol$^{-1}$, the value for migration of Si. That means that the formation of GP-II is a Si diffusion-controlled reaction. The addition of $Al_2O_3$ particles lowers the activation energy from 135 to 110 kJ mol$^{-1}$, equal to the activation energy for Mg diffusion. The reduction can be due to the extra dislocations acting as pipe-circuits for solute diffusion and/or the difference in the matrix composition. Mg is the excess alloying element in the MMC matrix.

The $Al_2O_3$ containing samples showed an acceleration of formation (peak C shifts to lower temperatures), but a reduction in the amount of $\beta'$ phase formed. The activation energy does not change. This might be attributed to the higher Mg content in the matrix of the composite. The excess Mg (the ratio of Mg : Si in the $\beta'$ phase is 1.68 [20]) in Al6061 makes the phase corresponding to peak C unstable [21]. Other factors may affect the height of peak C too, as the samples of Al6061 stored in the fridge seem to have the same effect on peak C. Whatever the mechanism, this observation shows that the relative proportions of $\beta''$ and $\beta'$ will be significantly different in an $Al_2O_3$/Al6061 composite when compared with Al6061. The addition of $Al_2O_3$ particles biases the formation of the $\beta''$, which contributes to strengthening, and hence increases the strength of the MMC.

The experimental findings in the storage time experiments can be explained by excess vacancy theory [22]. Upon quenching from 530 °C, excess vacancies may cluster to form small voids, and then collapse into vacancy loops. These kind of vacancy loops (pre-clusters) would serve as nuclei for precipitates. If the alloy is placed in a temperature regime (ageing) that allows stable growth of the pre-clusters, the excess vacancies will be incorporated in pre-clusters. As pre-clusters grow to a critical (stable) nucleus size, clusters or zones form. The critical stable nucleus size depends on the ageing temperature. Dutta found in transmission electron microscope (TEM) micrographs that the initial stage of ageing in an Al6061 is similar to that in Al–Si alloys [6]. Experiments on precipitation in the Al–Si alloy show that on ageing formation of vacancy loops decorated with Si atoms precedes the actual Si precipitation, which becomes detectable only after 2 h of ageing at about 130 °C [23]. It can be inferred that peak A in the DSC traces of the fresh samples of Al6061 reflects the formation of the vacancy loops. When a sample is stored in a fridge (about −5°C), vacancy loops decorated with solute atoms form and are of subcritical size. During a DSC run the pre-clusters continue to grow by vacancy-assisted solute atom clusters. The longer the delay, the larger the pre-cluster size. An increase in the pre-cluster size will result in an increase of the peak temperature [24]. If

this model is tenable, peak A in the DSC traces of the delayed samples would reflect the vacancy-assisted solute atom clusters. As vacancy-assisted solute cluster formation takes place during a DSC run, the supersaturation of solute remaining in solution is diminished. When the supersaturation is further reduced as a result of rising temperature, the size at which a cluster becomes stable is increased. Because supplies of solutes and vacancies from the matrix cannot support the growth of clusters, the clusters start to dissolve leading to peak A′. So it is suggested that the precipitation sequence in the delayed Al6061 is vacancy-assisted solute atom clusters (peak A), solute cluster dissolution (peak A′), GP-II formation (β″) (i.e. peak B), β′ formation (peak C) and β-$Mg_2Si$ formation (peak D). Further studies on the disappearance of GP-I formation in the delayed samples are needed.

## 4. Conclusions

1. Based on the DSC investigation, a precipitation sequence for Al6061, in the freshly water quenched state, is proposed as: (i) vacancy related clusters; (ii) competitive formation of GP-I and GP-II (β″) zones; (iii) precipitation of the β′ phase; (iv) formation of the β-$Mg_2Si$ phase.

2. The age-hardening sequences in the 20 vol % $Al_2O_3$/Al6061 are similar to those of the unreinforced Al6061 alloy.

3. The precipitation transformations of the metastable phases in both Al6061 and the composite obey a first-order kinetic model, with $0.9 < n < 1.2$.

4. The kinetic parameters for the formation of vacancy-related clusters, GP-I and GP-II (β″) zones, and β′ phase precipitates calculated using the varying heating method and the Kissinger expressions are in good agreement.

5. The addition of alumina particles reduces the amount of peaks A and C formed in Al6061 and shifts the peak temperatures to lower temperatures.

6. The addition of $Al_2O_3$ particles biases the formation of the β″, which contributes to the strengthening and will increase the strength of the composite.

## References


1. I. SINCLAIR and P. J. GREGSON, *Mater. Sci. Technol.* **13** (1997) 709.
2. H. J. RACK and R. W. KRENZER, *Metall. Trans.* **8A** (1977) 335.
3. J. M. PAPAZIAN, **19A** (1988) 2945.
4. A. K. GUPTA and D. J. LLOYD, in The Third International Conference on Al Alloys, pp. 21–26.
5. G. A. EDWARDS, K. STILLER, G. L. DUNLOP and M. J. COUPER, *Mater. Sci. Forum* **217–222** (1996) 713.
6. I. DUTTA and S. M. ALLEN, *J. Mater. Sci. Let.* **10** (1991) 323.
7. M. E. BROWN and C. A. R. PHILLPOTTS, *J. Chem. Edu.* **55** (1978) 556.
8. J. M. CRIADO, M. GONZALEZ, A. ORTEGA and C. REAL, *J. Thermal Anal.* **34** (1988) 1378.
9. J. ZSAKO, *ibid.* **34** (1988) 1489.
10. I. N. A. OGUOCHA and S. YANNACOPOULOS, *Mater. Sci. Engng* **A231** (1977) 25.
11. A. LUO, D. J. LLOYD, A. GUPTA and W. V. YOUDELIS, *Acta Metall.* **41** (1993) 769.
12. E. J. MITTEMEIJER, L. CHEN, P. J. VAN DER SCHAAF, C. M. BRAKMAN and B. M. KOREVAAR, *Metall. Trans.* **19A** (1988) 925.
13. E. J. MITTEMEIJER, *J. Mater. Sci.* **27** (1992) 3977.
14. J. DANIEL BRYANT, in "Automotive Alloys" edited by S. K. Das and G. J. Kipouros (The Minerals, Metals and Materials Society, London, 1997) pp. 19–36.
15. F. J. VERMOLEN, K. VUIK and S. VAN DER ZWAAG, *Mater. Sci. Engng* in press.
16. D. TURNBULL and R. L. CORIMA, *Acta Metall.* **8** (1960) 747.
17. M. TAYA, K. E. LULAY and D. J. LLOYD, *Acta. Metall. Mater.* **39** (1991) 73.
18. I. DUTTA and D. L. BOURELL, *ibid.* **38** (1990) 2041.
19. S. K. PABI, *Mater. Sci. Engng* **43** (1980) 151.
20. K. MATSUDA, S. TADA, S. IKENO, T. SATO and A. KAMIO, in Proceedings of the Fourth International Conference on Al Alloys, Atlanta, GA (1994) pp. 598–604.
21. M. TAKEDA, F. OHKUBO, T. SHIRAI and F. FUKUI, *Mater. Sci. Forum* **217–222** (1996) 815.
22. B. CHARMERS, *Progress Mater. Sci.* **10** (1963) 172.
23. P. VAN MOURIK, E. J. MITTEMEIJER and T. H. KEIJSER, *J. Mater. Sci.* **18** (1983) 2706.
24. J. M. PAPAZIAN, *Metall. Trans.* **13A** (1982) 761.



*Received 9 April*
*and accepted 22 June 1998*